Journal of Fluids and Structures 27 (2011) 668–679

Contents lists available at ScienceDirect

Journal of Fluids and Structures

journal homepage: www.elsevier.com/locate/jfs

Flows past rotating cylinders next to a wall

A. Rao [a], B.E. Stewart [a], M.C. Thompson [a], T. Leweke [b], K. Hourigan [a,c,*]

[a] Fluids Laboratory for Aeronautical and Industrial Research (FLAIR), Department of Mechanical and Aerospace Engineering, Monash University, Clayton 3800, Australia
[b] Institut de Recherche sur les Phénomènes Hors Équilibre (IRPHÉ), CNRS/Universités Aix-Marseille, 49 rue Frédéric Joliot-Curie, B.P. 146, F-13384 Marseille Cedex 13, France
[c] Division of Biological Engineering, Monash University, Clayton 3800, Australia

ARTICLE INFO

Article history:
Received 19 October 2010
Received in revised form
21 March 2011
Accepted 25 March 2011
Available online 20 May 2011

Keywords:
Rotating bodies
Stability analysis
Wakes
Body forces
Flow transition

ABSTRACT

Two-dimensional simulations are used to investigate the flow past rotating circular cylinders near a wall in the low Reynolds number regime ($20 \leq Re \leq 750$). For the single cylinder case, rotation rates higher than previously studied are considered. For cylinders rolling forward, the wake flow structures observed are similar to those seen in previous studies; however, it is found that reverse rotation of the cylinder can completely suppress vortex shedding. The drag force on the cylinder is quantified. Linear stability analysis is used to determine the onset of three-dimensionality in the wake. Increased forward rotation triggers three-dimensionality at increasingly lower Reynolds numbers, while reverse rotation delays this transition to much higher values. For the highest reverse rotation rate, three-dimensionality was suppressed at the higher end of the Reynolds number range investigated. A study of two sliding cylinders is also performed, especially focusing on the interaction of the first wake with the second, the effect on the overall wake dynamics and quantification of the drag on each cylinder.

1. Introduction

The separated flow over a circular cylinder is one of the classical fluid dynamics problems, studied in detail for over a century since the pioneering investigations of Bénard (1908) and von Kármán (1911). Since then, there have been many comprehensive review articles, including Williamson (1996a,b), Norberg (2003), and reviews of wake transition for other cylindrical or axisymmetric bluff bodies (e.g., Thompson et al., 2006b). The flow dynamics are dramatically altered when such bodies are placed close to a plane wall. A significant change in shedding frequency and forces experienced by these bodies is observed, compared with similar bodies in an unbounded flow. An added parameter to such investigations is the effect of body rotation. By use of a numerical solver, we examine the flow structures and wake dynamics, and compute the forces on a circular cylinder as a function of rotation rate and Reynolds number, and then extend this study to examine two sliding cylinders.

One motivation for this study is to improve our understanding of the flow dynamics of, and forces on, cells near blood vessel walls of which the current problem is a simplified two-dimensional analogue. Certain cell types such as platelets and leukocytes depend on rolling and sliding along a vessel wall as part of the activation process to initiate the clotting or

* Corresponding author at: Fluids Laboratory for Aeronautical and Industrial Research (FLAIR), Department of Mechanical and Aerospace Engineering, Monash University, Clayton 3800, Australia.
E-mail address: Kerry.Hourigan@monash.edu (K. Hourigan).

0889-9746/$ - see front matter © 2011 Elsevier Ltd. All rights reserved.
doi:10.1016/j.jfluidstructs.2011.03.019

immune response (Lawrence and Springer, 1991; Wagner and Frenette, 2008). This study is a prelude to studies investigating flow behaviour at much lower Reynolds numbers, which may be directly applicable to the above mentioned examples. The current study is also applicable to many particle–particle and particle–wall interactions, (e.g., particles in a sedimentation tank), as it considers a wider parameter range.

2. Flows around a single cylinder close to a plane wall

The effect of placing a body in close proximity to a wall brings about a substantial change to the wake flow structure and consequently the forces experienced by the body, compared with an unbounded flow. Investigations in a wind tunnel by Bearman and Zdravkovich (1978) showed a strong suppression of vortex shedding for a gap to diameter ratio $G/D=0.3$, for a cylinder adjacent to a stationary wall. The lift force experienced by the cylinder was directed away from the wall for the cases investigated but the Strouhal number (St) remained approximately constant as the cylinder moved closer towards $G/D=0.3$.

A single row of vortices was observed by Taneda (1965) for a cylinder moving close to a wall at $\mathrm{Re}=170$. The experiments were conducted using condensed milk and aluminium dust to visualise the vortex structures. It was noted that the time period for the vortex formation was longer than that in free stream.

Lei et al. (2000) investigated the effect of gap ratio (G/D) between 0.1 and 3 for a Reynolds number range of 80–1000. Using a finite-difference method, they describe the flow structure formation behind the cylinder for $G/D<3$. The lower wall is stationary, leading to the formation of a boundary layer, which interacts with the shear layer shed from the lower side of the cylinder. At different gap ratios and Reynolds numbers, the opposite signed vorticity in the wall shear layer and the shear layer shed from the cylinder cancel each other out, leading to the suppression of vortex shedding. It was also found that the critical gap ratio at which the shedding ceases decreases with an increase in Reynolds number, asymptoting to 0.2 at higher values.

Nishino et al. (2007) conducted experiments in a wind tunnel for intermediate Reynolds numbers $O(10^5)$ with a moving wall to prevent the development of a boundary layer. Three regions of vortex shedding based on the gap height were identified. For $G/D>0.5$, regular vortex shedding was observed; and as the cylinder was moved closer to the wall, the shedding became intermittent and ceased to exist for gap ratios ≤ 0.35. The experiments showed a decrease in drag coefficient as the cylinder was moved progressively closer to a wall, becoming constant for $G/D\leq 0.35$.

Numerical simulations for a stationary cylinder close to a moving wall have been performed by Huang and Sung (2007). They obtained a critical vortex suppression value of $G/D=0.28$, which is close to that observed for simulations conducted with a stationary wall. Furthermore, they attributed the formation of the vortex from the lower side of the cylinder to the higher flow rate between the cylinder and the moving wall. For a constant gap ratio, the lift and drag values increased as the Reynolds number was increased from 200 to 500. Numerical simulations have also been carried out for rotating bodies close to a stationary wall. Using the lattice Boltzmann method, Cheng and Luo (2007) obtained flow structures and quantified the forces on a rotating cylinder near a stationary wall. The magnitude and sense of rotation affect the critical height at which vortex shedding is suppressed. For a given gap ratio, the lift coefficient increased as the rotation rate was changed from retrograde to prograde, while the drag coefficient showed the reverse trend.

Two- and three-dimensional studies for a square cylinder near a stationary wall have been conducted by Mahir (2009). The mean drag force decreased as the cylinder was brought close to a wall. It was also noted that the two-dimensional simulations overpredicted the mean lift and drag values. Their simulations considered a body adjacent to a stationary wall, while the present work focuses on a body in motion along a plane surface.

Stewart et al. (2010) conducted two- and three-dimensional numerical simulations for a single cylinder rolling along a wall. The gap ratio was maintained at 0.005 to prevent the grid singularity that occurs if the cylinder is touching the wall. Forward rolling of the cylinder destabilised the flow, reducing the Reynolds number at which shedding first occurred, while reverse rolling stabilised it. The lift and drag values were found to be highly dependent on the rotation rates. The steady and unsteady regimes of the flow for different rotation rates were mapped. In the unsteady regime, the shear layer shed from the top of the cylinder combined with the wall shear layer downstream, forming a vortex pair with a net rotation. Their stability analysis reported that the wake undergoes a transition to three-dimensionality and then becomes unsteady, as the Reynolds number is increased. The transition mechanism to three-dimensionality was not clearly understood. Experimental work carried out in a water channel confirmed the flow features visualised in the numerical simulations. The current work is an extension of that study: first to higher forward and reverse rotation rates and then to multiple circular cylinders.

3. Problem definition and methodology

This study is an extension to the generic flow problem of a single cylinder rolling, without slipping, along a wall in a quiescent fluid. That problem is governed by a single parameter, the Reynolds number $\mathrm{Re}=UD/\nu$, where D is the cylinder diameter, U the velocity of its centre, and ν the kinematic viscosity of the fluid. In the general case, in which slip between the cylinder and the wall is allowed, another parameter is needed to fully describe the flow. A convenient choice is the rotation speed at the cylinder surface relative to the linear speed at its centre $\alpha=(\omega D/2)/U$, where ω is the angular velocity. Forward rolling (i.e., rotation against the flow at the top of the cylinder—anti-clockwise in this case) corresponds

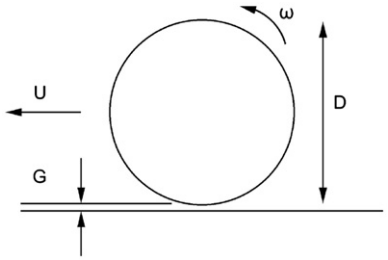

Fig. 1. Schematic representation of the cylinder.

to positive α values, and reverse rolling (i.e., aiding the flow or clockwise) corresponds to negative α values. The range of Reynolds numbers considered in this study is between 20 and 200 for $\alpha \geq 0$ and between 20 and 750 for $\alpha < 0$. In the current study, α is varied between -2 and $+2$. A schematic representation of the rolling cylinder is shown in Fig. 1. The cylinders are placed at a very small distance above the wall to prevent the formation of singular elements directly beneath the cylinders. The gap height normalised by the cylinder diameter, G/D, is set to 0.005. Previous studies (Stewart et al., 2006, 2010) have shown that the simulated flow structures match the experimentally observed ones when the cylinder is actually in contact with the wall, although it is true that the lift and drag forces are sensitive to the gap ratio. At low Reynolds numbers, the drag force was more sensitive to the gap ratio than at higher flow speeds. The frequency of shedding of the wake, f, is quantified through the non-dimensional Strouhal number, $\mathrm{St} = fD/U$. The drag coefficient (per unit width) reported here is given by $\overline{C_d} = \overline{F_d}/(\frac{1}{2}\rho U^2 D)$, where $\overline{F_d}$ is the time-averaged force experienced by the cylinder. Visualisations for all cases presented here are with flow from left to right in the frame of reference of the cylinder. Vortical structures have been visualised using a red/blue colour scheme, where red indicates negative, and blue positive vorticity, respectively. The contour levels for all figures shown are between $\pm 5U/D$.

3.1. Numerical formulation

In order to compute the flow numerically, the incompressible Navier–Stokes equations are solved in the frame of reference of the cylinder. In this inertial reference frame, the fluid moves from left to right at constant speed U. A detailed description of the numerical method and implementation is given in Thompson et al. (2006a); it has previously been employed to investigate bluff body flow dynamics for many related problems, e.g., Stewart et al. (2010), Thompson et al. (1996), Thompson et al. (2001), Leontini et al. (2007), Tan et al. (2005), Le Gal et al. (2001). The numerical method uses the spectral-element approach with the computational domain constructed from a set of quadrilateral elements with curved sides as necessary to accurately model the cylinder surface. Each element is further sub-divided by a set of internal nodes distributed according to the Gauss–Legendre–Lobatto quadrature points, with the velocity and pressure fields represented by a tensor product of Lagrangian polynomial interpolants within the elements. While the method is only continuous in the function, and not in the derivatives, across element boundaries, it has been shown to provide spectral or exponential convergence as the interpolant order is increased (Karniadakis and Sherwin, 2005). A key advantage with the method is the ability to specify the number of nodes per element $N \times N$ at runtime. The interpolant polynomial order is then given by $N-1$. The fractional step technique is used for the time integration (Chorin, 1968; Karniadakis et al., 1991) for computing both the steady and unsteady wakes.

At the solid boundaries and the inflow and top domain boundaries, the velocity was set to the relevant known values to provide the boundary conditions there. At the outflow boundary, the pressure was set to zero together with the normal velocity gradient. The domain boundaries were placed at sufficiently large distances from the cylinder to reduce blockage to about 1%.

3.2. Linear stability analysis

The transition to three-dimensionality in the wake forms an important aspect of understanding flows over bluff bodies, not least because it precedes the transition to fully turbulent flow, and the remnants of these three-dimensional modes tend to persist into the fully turbulent regime (Williamson, 1996b; Wu et al., 1996). Flows over bodies moving close to the ground have been found to undergo transition to three-dimensionality before becoming unsteady, as shown by Stewart et al. (2010), which is noted to be similar to the three-dimensional transition for flow over a backward-facing step (Barkley et al., 2002). In order to determine the transitional values, we perform linear stability analysis by splitting the velocity and pressure fields into two-dimensional components describing the stable or unstable base flow plus three-dimensional perturbations. Mathematically, the linearised Navier–Stokes equations for the perturbation fields admit solutions based on exponential growth or decay in time, together with sinusoidal variation in the spanwise direction. In general, the full solution can be constructed as a Fourier sum of spanwise modes, each growing or decaying exponentially in time. In practice, for each Reynolds number and each spanwise wavelength (λ), the linearised equations can be integrated in time

Table 1
Variation of the time-averaged drag coefficient for $\alpha = +2$.

N	Re = 20		Re = 200	
	$\overline{C_d}$	Variation (%)	$\overline{C_d}$	Variation (%)
4	10.295424	−9.063091	3.920135	−2.507025
5	11.210904	−0.976885	4.027608	0.165807
6	11.281302	−0.355077	4.022211	0.031585
7	11.273864	−0.420775	4.015624	−0.132233
8	11.311096	−0.091914	4.024288	0.083239
9	11.321852	0.003091	4.021998	0.026287
10	11.321418	−0.000742	4.018557	−0.059290
11	11.321502	0	4.020941	0

Table 2
Variation of the time-averaged drag coefficient for $\alpha = -2$.

N	Re = 20		Re = 750	
	$\overline{C_d}$	Variation (%)	$\overline{C_d}$	Variation (%)
4	9.375690	3.380668	0.228723	−4.688425
5	9.134668	0.723049	0.241246	0.530057
6	9.087320	0.200968	0.240163	0.078759
7	9.084586	0.170822	0.240082	0.045005
8	9.072538	0.037975	0.239991	0.007084
9	9.069034	−0.000662	0.239969	−0.002084
10	9.069136	0.000463	0.239973	−0.000417
11	9.069094	0	0.239974	0

starting from a base flow perturbed with white noise. After some time, for each spanwise wavelength, only the dominant instability mode remains, since it is the one that grows fastest or decays most slowly. In fact, it is possible to extract the first few most important modes for each spanwise wavelength by using an Arnoldi decomposition of the snapshots of the evolving fields at fixed time intervals (T), typically the base flow period if the base flow is periodic (see, e.g., Barkley and Henderson, 1996; Ryan et al., 2005). In that case, the instability analysis is called Floquet analysis. The growth rate (σ) of each mode can be related to the amplification factor (μ) over time T by $\mu = e^{\sigma T}$. The critical Reynolds number ($\mathrm{Re_c}$), corresponding to a maximum growth rate of $\sigma = 0$ or amplification factor $\mu = 1$, over all wavelengths, marks the transition to three-dimensional flow. For the case of rolling cylinders near a wall, the flow is steady before the onset of three-dimensionality, unlike the case of a cylinder in an unbounded flow, where three-dimensionality develops on an already unsteady periodic base flow (Thompson et al., 1996; Barkley and Henderson, 1996). More details of the theory and numerical approach can be found, e.g., in Griffith et al. (2007), Leontini et al. (2007) and Ryan et al. (2005).

3.3. Domain size and mesh resolution studies

The computational domain chosen was of similar dimensions to that used for previous work, with the inlet and outlet at $100D$ upstream and downstream of the cylinder, and the top boundary placed $150D$ from the wall. The spatial resolution is controlled by varying the number of interpolation points in each direction, N. These points are used as a basis for constructing the Lagrange interpolating polynomials over which integration is carried out, as described above. The number of points over each (two-dimensional) element was varied between $N^2 = 16$ and 121. This check was carried out for the two extreme cases of the Reynolds number at the maximum rotation rates of $\alpha = \pm 2$. Tables 1 and 2 tabulate the drag coefficient as the spatial resolution is increased. For $N = 8$, the values are within 0.1% of the maximum tested resolution. Furthermore, at $N = 8$, the Strouhal number at Re = 200 and $\alpha = +2$ was well within 0.2% of that at the maximum tested resolution.

4. Results

4.1. Flow structures

Initially, we focus on the wake flow structures for different rotation rates. For moderate Reynolds numbers and for positive α, the shear layer rolls up behind the cylinder forming a strong clockwise vortex, which grows in strength prior to eventually detaching from the separating shear layer. This vortex induces the generation of vorticity of opposite sign beneath it in order to satisfy the no-slip boundary condition there. For the Reynolds number shown (Re = 180), diffusion is

low enough to allow the secondary vorticity to be pulled away from the wall to form a vortex pair, which subsequently self-propels away from the wall through self-induction. This same scenario is observed for all positive rotation rates examined, as shown in Fig. 2. Although the parameter space was generally restricted to $\alpha = \pm 2$, some visualisations were carried out at a higher rotation rate of $\alpha = +3$. The vortex formed at the top of the cylinder rolls up in a more circular shape at higher rotation rates as compared to $\alpha = 1$, where a more oblate vortex pair is formed. Also, the increased rotation rate moves the separation point of the separating shear layer further forward. The transition from steady state to unsteady flow was found to occur at lower Reynolds numbers when increasing the rotation speed. Vortex shedding was observed at $Re = 65$ at $\alpha = +2$, in contrast to unsteady flow being first observed at $Re \geq 90$ and 160 for $\alpha = +1$ and 0, respectively. The flow at these Reynolds numbers is three-dimensional and unsteady; the flow structures have two-dimensional projections resembling the computed two-dimensional wakes shown here, but with an additional spanwise waviness (see Stewart et al., 2010).

Vortex shedding was found to occur only at higher Reynolds numbers ($Re \geq 425$) for a cylinder in clockwise rotation or reverse rolling ($\alpha = -1$) (Stewart et al., 2010). In Fig. 3, wakes are shown for $Re = 750$. The vortex pairs formed in this case drifted farther away from the wall at this flow speed, compared with those at $Re = 450$. On increasing the rotation speed in the clockwise direction to $\alpha = -1.25$, vortex shedding was detected only for $Re > 700$. The structure of the shear layers formed behind the cylinder resembled that at $\alpha = -1$. The frequency of shedding was far higher and the vortex structures formed were much smaller compared to those at $\alpha = -1$, and they remained closer to the wall. On further increasing the magnitude of (negative) rotation speed, the flow structure changed dramatically and vortex shedding ceased to occur for $Re \leq 750$ and $\alpha = -2$. A stand-alone run for $\alpha = -3$ showed that vortex shedding continued to be suppressed at higher negative rotation rates. For these very high reverse rotation rates, the cylinder boundary layer wraps all the way around the cylinder, almost preventing separation entirely. Note that for a rotating cylinder in a free stream, vortex shedding is briefly suppressed between rotation rates of $1.91 \leq \alpha \leq 4.34$ and beyond $\alpha \geq 4.8$ (Mittal and Kumar, 2003).

Stages of vortex shedding for $\alpha = +2$ at $Re = 200$ are shown in Fig. 4 for one time period, along with the corresponding instances on the force history diagram. Points (a) and (e) both correspond to image (a). At $\tau = 165$, the vortex pair behind the rolling cylinder is about to drift away from the cylinder wall system. At a slightly later time of $\tau = 170$ [image (b)],

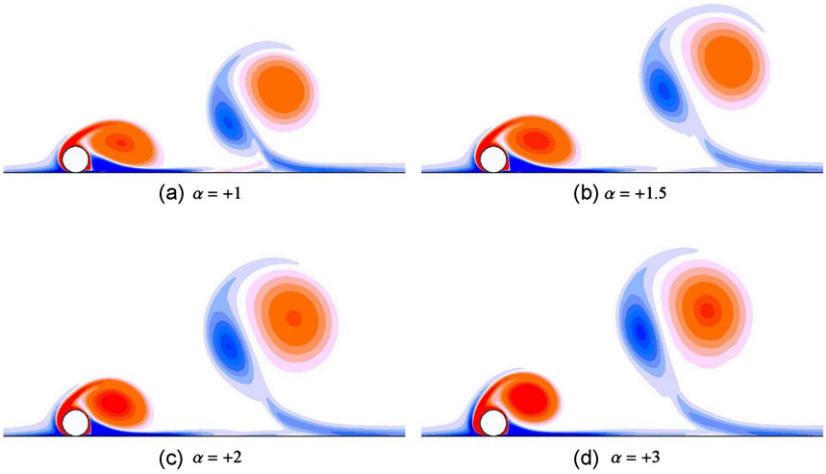

Fig. 2. Evolution of the wake for the anti-clockwise rotation of a single cylinder at $Re = 180$ for the rotation rates shown. Vorticity contours and colours are the same in all images. The vortex pair for $\alpha = +3$ is the strongest. (For interpretation of the references to colour in this figure legend, the reader is referred to the web version of this article.)

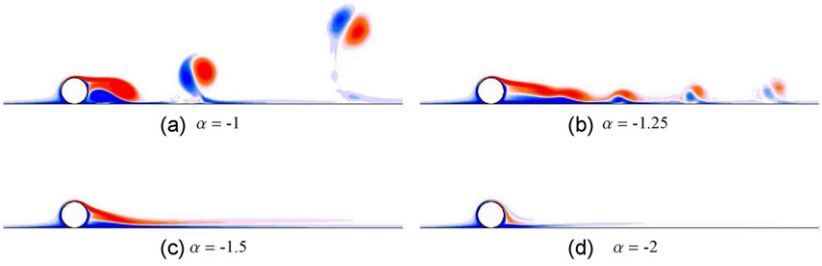

Fig. 3. Evolution of the wake for the clockwise rotation of a single cylinder at $Re = 750$ for the rotation rates shown.

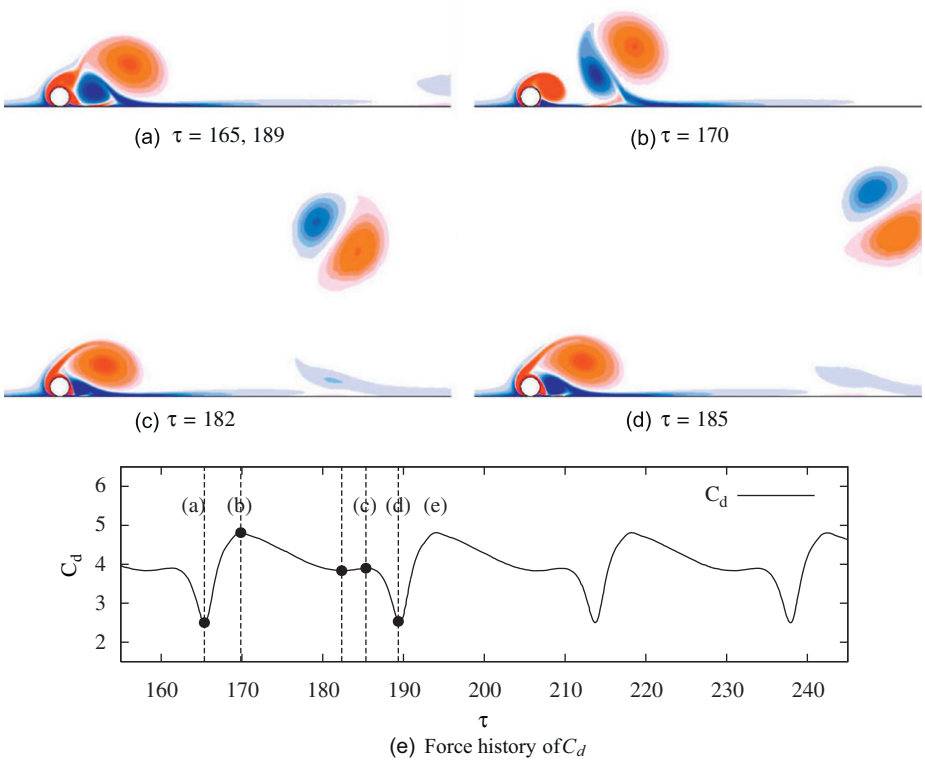

Fig. 4. (a–d) Vorticity snapshots for the single cylinder rolling at $\alpha = +2$ and Re=200. (e) Instantaneous drag coefficient (C_d).

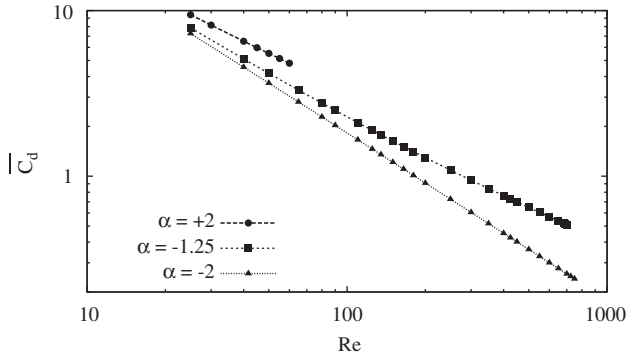

Fig. 5. Variation of the drag coefficient for different rotation rates in the steady state regime.

we observe that the drag has almost doubled, due to the low pressure caused by the rolling up of the shear layer above the cylinder. The vortex grows larger and moves away from the cylinder, leading to the recovery of pressure, thereby causing a drop in the drag force until $\tau = 182$ [image (c)]. As explained previously, the wall shear layer is also being drawn up by the much larger vortex from the top of the cylinder and leads to a slight increase in drag force [image (d)]. At a slightly later stage, the shear layer on the top of the cylinder has rolled up and has drifted further away, and a decrease in drag is observed.

4.2. Drag and Strouhal number trends

Drag coefficients for the steady and unsteady cases are shown in Figs. 5 and 6, respectively. For the steady cases, we observe that the trends vary linearly on a log–log plot. These trends are similar to those previously observed by Stewart et al. (2010) for cylinders at lower rotation rates.

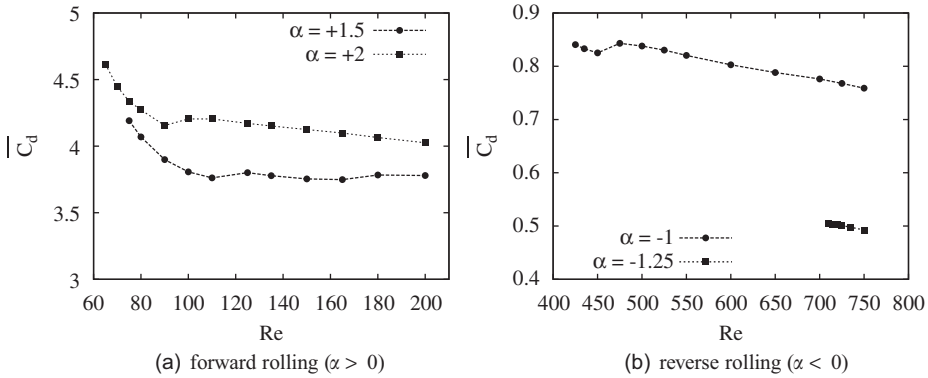

Fig. 6. Variation of the time-averaged drag coefficient with Reynolds number in the unsteady regime.

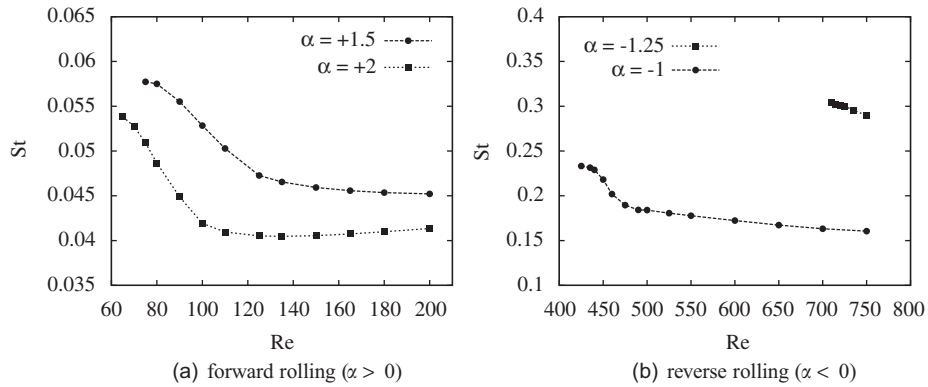

Fig. 7. Strouhal–Reynolds number relationships.

The Strouhal number variation for the higher rotation rate cases investigated is shown in Fig. 7. Strouhal numbers for the negative rotation rates are much higher compared with the positive rotation cases.

4.3. Three-dimensional transition

Stability analysis was conducted to determine the critical Reynolds number at which the flow undergoes transition to three-dimensional flow. As described above, linear stability analysis is performed based on two-dimensional steady or unsteady base flows. In practice, this amounts to determining the growth rates of the dominant modes corresponding to a range of spanwise wavelengths, for a set of Reynolds numbers. The aim is to determine the critical Reynolds number at which the growth rate first becomes zero, and the corresponding wavelength.

For the simulations conducted here, three-dimensionality is initially triggered on the steady base flow at Reynolds numbers less than the values at which unsteady flow occurs, in agreement with the findings of Stewart et al. (2010). Fig. 8 presents plots of growth rate as function of axial wavelength for different rotation rates. Fig. 9 summarises the results from the analysis of these curves: the variation of the critical Reynolds number and wavelength with rotation rate. As the rotation is increased from $\alpha = -1.5$ to $+2$, the transition Reynolds number monotonically decreases, while the critical spanwise wavelength monotonically increases.

4.4. Comparison with experimental results

Experiments were performed in a water tunnel using a cylinder driven by a stepper motor placed adjacent to a purpose-built moving floor, as described in Stewart et al. (2006, 2010). Some dye visualisations showing the two-dimensional structure of the wake for different rotation rates are shown in Figs. 10–12. Note that these images are taken just after startup, before the wake has become too three-dimensional, both from end-effects given the short aspect ratio (13:1), and the growth of the intrinsic three-dimensional instability as discussed above. The corresponding numerical simulations were conducted at slightly higher Reynolds numbers than for the experiments. This is because unsteady transition is triggered at subcritical Reynolds numbers with the current experimental setup.

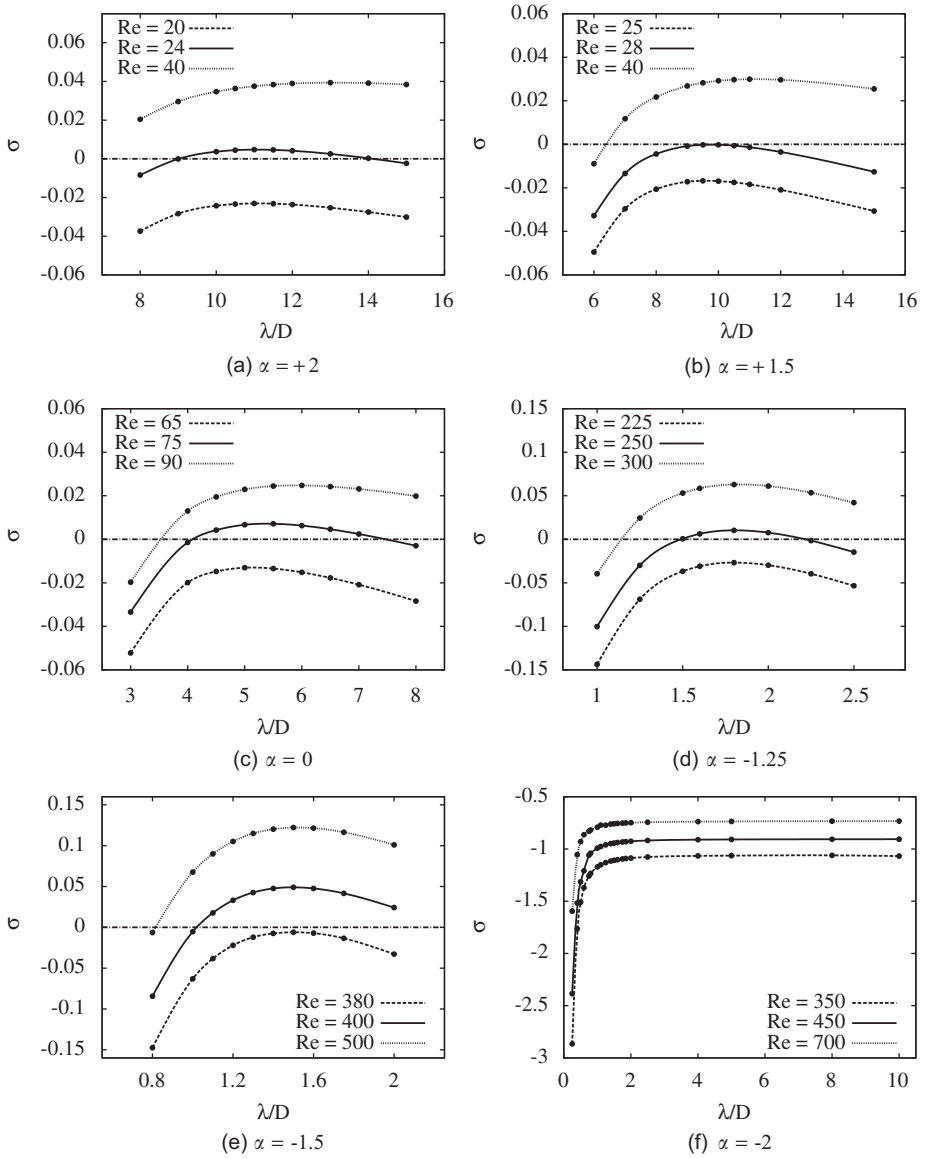

Fig. 8. Variation of growth rate for different rotation rates.

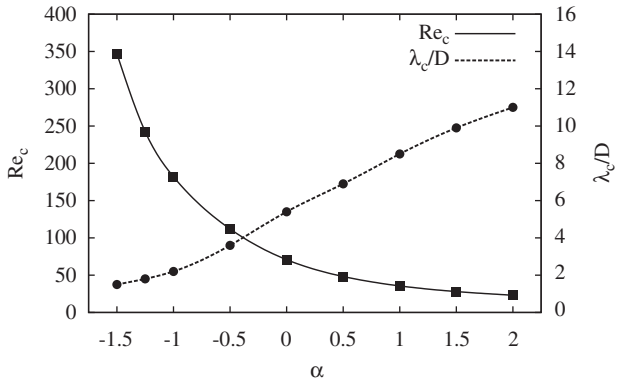

Fig. 9. Variation of the critical Reynolds number and wavelength with rotation rate, extending the work of Stewart et al. (2010).

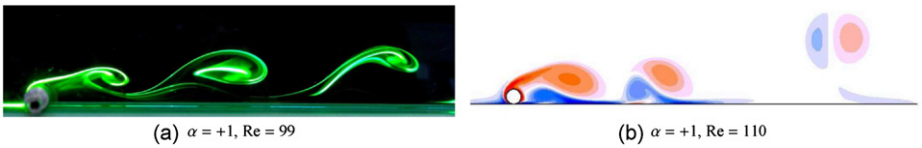

Fig. 10. Dye visualisations from the water channel (left) and vorticity contours from the numerical simulations (right).

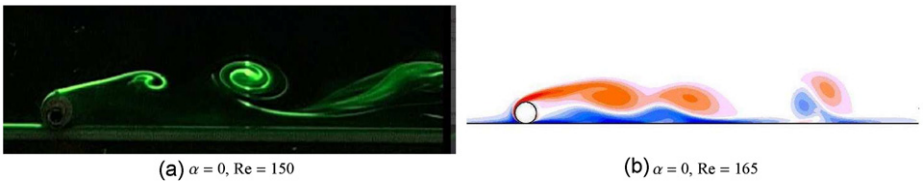

Fig. 11. Dye visualisations from the water channel (left) and vorticity contours from the numerical simulations (right).

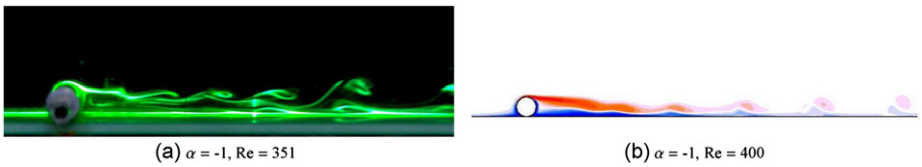

Fig. 12. Dye visualisations from the water channel (left) and vorticity contours from the numerical simulations (right).

Fig. 13. Schematic representation of the tandem cylinder.

5. Tandem cylinders

The flow characteristics of a bluff body are altered when a body of similar dimension is placed in its vicinity (see, e.g., Sumner, 2010 for a recent review). Here, we consider the case of two-dimensional flow around two cylinders sliding along a plane wall without rotation ($\alpha = 0$). The trailing body is placed downstream of the first body at different normalised separation distances (S/D), measured as the dimensionless distance between the cylinders (see Fig. 13). As for the case of a single cylinder, a gap of size $G/D = 0.005$ is maintained between the cylinders and the wall. The range of Reynolds numbers for this investigation is 20–200 and the separation distance is varied between $0.1 \leq S/D \leq 10$. One motivation for this study comes from the drag reduction of the trailing or the downstream body when placed at close separation distances. At very large spacings, the cylinders effectively behave as individual entities and the flow characteristics of both should resemble those of a single cylinder.

The numerical formulation and the problem setup are very similar to that for a single cylinder. However, there is an increase in the number of macro-elements required in order to resolve the boundary layers of each cylinder and the larger region with high velocity gradients, which leads to the increase in computational effort. Mesh resolution studies were also carried out for the case of $S/D = 10$. A domain size of $50D$ (inlet) $\times 50D$ (top surface) $\times 100D$ (outlet) was used for the simulations, with the outlet boundary being placed $100D$ from the downstream cylinder, and a polynomial order $N = 7$. This was sufficient to capture the drag force accurately.

It may be recalled that the critical value for transition to unsteady state for a single cylinder sliding along a wall is Re = 160 (Stewart et al., 2010). In general for the tandem cylinder case, the flow was found to become more stable as (a) the Reynolds number decreased and (b) as the separation distance between the two cylinders decreased. For example, at Re = 200, the maximum Reynolds number tested, the flow was steady only for spacings $S/D \leq 4.5$. However, decreasing Re to 180, the flow remained steady out to spacings $S/D = 6$ (Fig. 14). Further decreasing the Reynolds number to Re = 150, unsteady flow was still detected but only for spacings greater than $S/D = 8$. Compared with the single cylinder sliding case,

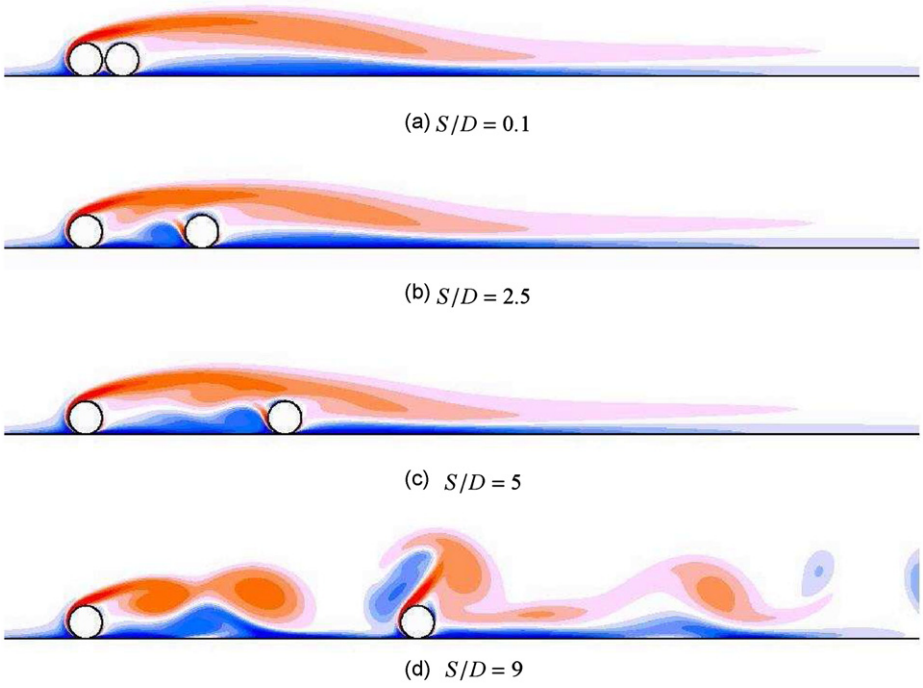

Fig. 14. Instantaneous flow structures at Re=180, as the spacing ratio S/D is increased. Vortex shedding is seen for S/D=9.

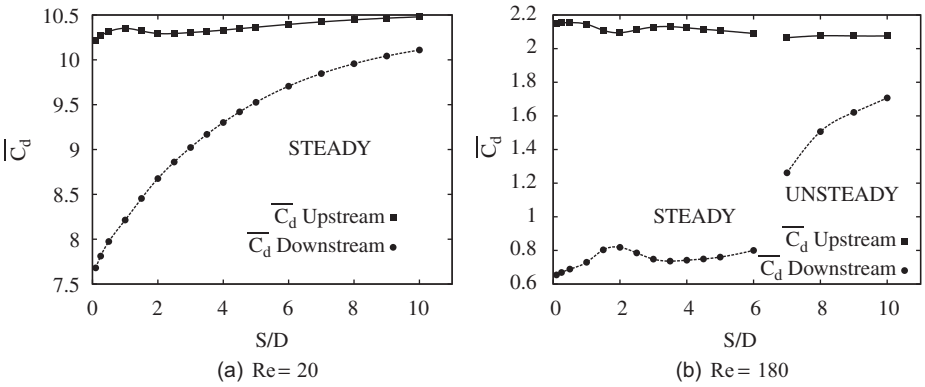

Fig. 15. Variation of the time-averaged drag coefficient with separation distance at the specified Reynolds numbers.

the presence of a downstream cylinder thus provides a stabilising effect (i.e., increases the transitional Reynolds number) on the wake for closer separation distances but destabilises the flow for greater separation distances.

The variation of the upstream and downstream cylinder drag coefficients with respect to separation distance is shown for Reynolds numbers 20 and 180 in Fig. 15. The drag on the downstream cylinder increases as the spacing between the cylinders is increased. A more rapid rise is observed for cases where the transition to unsteady state occurs. At the higher Reynolds number, the drag on the downstream cylinder for small separations is low, but remains positive. This is in contrast to the free-stream case, where the downstream cylinder experiences negative drag force at very close spacings. Fig. 16 shows the pressure distribution for the tandem cylinders at the closest spacing of S/D=0.1 at Re=200. The higher pressure near the wall on the upstream face of the downstream cylinder, together with the lower pressure on the downstream face, leads to a positive drag force.

The drag variation of the two cylinders with Reynolds number is shown in Fig. 17 for three separation distances. Only at very large spacings, the drag on the downstream cylinder approaches that of the upstream cylinder.

On increasing the separation distance, multiple circulation regions were formed in the space between the sliding cylinders, as shown for a particular case in Fig. 18.

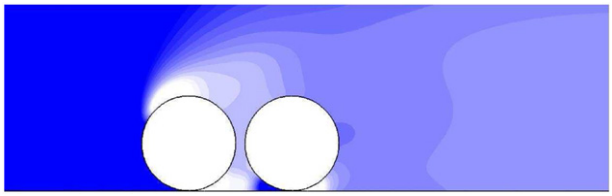

Fig. 16. Pressure distribution for cylinders separated by $S/D=0.1$ at $\mathrm{Re}=200$. The darker shades indicate a higher pressure region, while the lighter shades indicate regions of lower pressure.

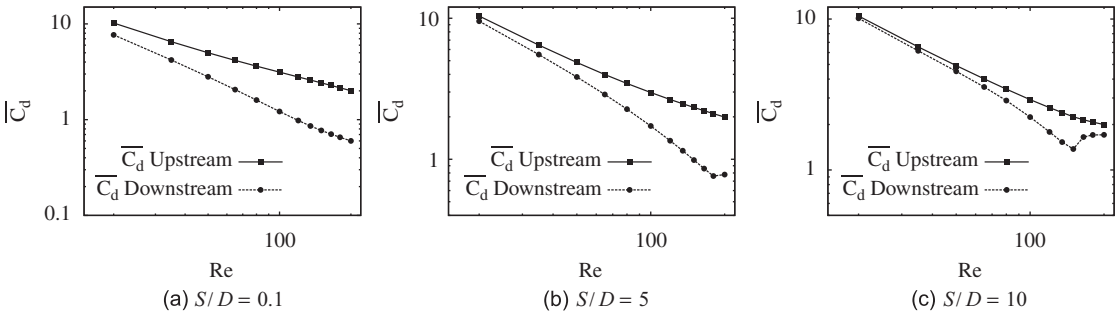

Fig. 17. Variation of the time-averaged drag coefficient with Reynolds number for the separation distances shown.

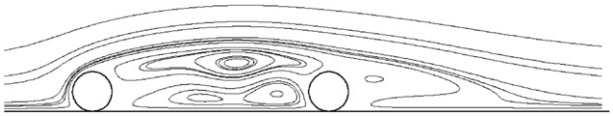

Fig. 18. Streamlines for $S/D=5$ at $\mathrm{Re}=180$. Formation of multiple recirculation zones in the space between the two cylinders.

6. Conclusions

This paper extends the results for a single rotating cylinder close to contact with a plane wall to higher rotation rates than previously considered. For the forward rolling case, wake flow structures at rotation rates up to $\alpha=3$ were found to be similar to those for lower rotation rates, except for the strength of the vortex pairs which self-propel away from the wall. This can be understood in terms of the velocity difference across the wake, which results in a higher flux of vorticity into the separating shear layer and subsequently stronger shed vortices. For the reverse-rotating case, the fluid boundary layer effectively remains attached as it passes over the surface of the cylinder. For $\alpha<-1.25$, vortex shedding is suppressed up to at least $\mathrm{Re}=700$. In addition, high reverse rotation also stabilises the flow against three-dimensional instability. For both forward and reverse rotation, the drag experienced by the cylinder has been quantified. This paper also presents results for a pair of cylinders sliding along a plane wall, as a function of separation distance. Overall, the presence of the second cylinder results in the delay of transition to unsteady flow to higher Reynolds numbers. The drag on the downstream cylinder increases after the onset of unsteady flow.

Acknowledgements

The support from Australian Research Council Discovery Grants DP0877327 and DP0877517 and computing time from the National Computational Infrastructure Facility (NCI), Victorian Life Sciences Computation Initiative (VLSCI) and Monash Sungrid are gratefully acknowledged. Anirudh Rao acknowledges the support of a Monash University Departmental Postgraduate Scholarship. Bronwyn Stewart acknowledges the support of an Australian Postgraduate Award and of a Mobility Grant from the French Ministry of Higher Education and Research.

References

Barkley, D., Gomes, M.G.M., Henderson, R.D., 2002. Three-dimensional instability in flow over a backward-facing step. Journal of Fluid Mechanics 473, 167–190.

Barkley, D., Henderson, R.D., 1996. Three-dimensional Floquet stability analysis of the wake of a circular cylinder. Journal of Fluid Mechanics 322, 215–241.

Bearman, P.W., Zdravkovich, M.M., 1978. Flow around a circular cylinder near a plane boundary. Journal of Fluid Mechanics 89, 33–47.

Bénard, H., 1908. The formation of gyration centres at the back of a moving obstacle. Comptes Rendus Hebdomadaires des Séances de l'Académie des Sciences 147, 839.
Cheng, M., Luo, L.S., 2007. Characteristics of two-dimensional flow around a rotating circular cylinder near a plane wall. Physics of Fluids 19, 063601.
Chorin, A.J., 1968. Numerical solution of the Navier–Stokes equations. Mathematics of Computation 22, 745–762.
Griffith, M.D., Thompson, M.C., Leweke, T., Hourigan, K., Anderson, W.P., 2007. Wake behaviour and instability of flow through a partially blocked channel. Journal of Fluid Mechanics 582, 319–340.
Huang, W.X., Sung, H.J., 2007. Vortex shedding from a circular cylinder near a moving wall. Journal of Fluids and Structures 23, 1064–1076.
von Kármán, T., 1911. Über den Mechanismus des Widerstandes, den ein bewegter Körper in einer Flüssigkeit erfährt. Göttinger Nachrichten Mathematisch-Physikalische Klasse 12, 509–517.
Karniadakis, G.E., Israeli, M., Orszag, S.A., 1991. High-order splitting methods for the incompressible Navier–Stokes equations. Journal of Computational Physics 97, 414–443.
Karniadakis, G.E., Sherwin, S.J., 2005. Spectral/hp Methods for Computational Fluid Dynamics. Oxford University Press, Oxford.
Lawrence, M.B., Springer, T.A., 1991. Leukocytes roll on a selectin at physiologic flow rates: distinction from and prerequisite for adhesion through integrins. Cell 65, 859–873.
Le Gal, P., Nadim, A., Thompson, M., 2001. Hysteresis in the forced Stuart–Landau equation: application to vortex shedding from an oscillating cylinder. Journal of Fluids and Structures 15, 445–457.
Lei, C., Cheng, L., Armfield, S., Kavanagh, K., 2000. Vortex shedding suppression for flow over a circular cylinder near a plane boundary. Ocean Engineering 27, 1109–1127.
Leontini, J.S., Thompson, M.C., Hourigan, K., 2007. Three-dimensional transition in the wake of a transversely oscillating cylinder. Journal of Fluid Mechanics 577, 79–104.
Mahir, N., 2009. Three-dimensional flow around a square cylinder near a wall. Ocean Engineering 36, 357–367.
Mittal, S., Kumar, B., 2003. Flow past a rotating cylinder. Journal of Fluid Mechanics 476, 303–334.
Nishino, T., Roberts, G.T., Zhang, 2007. Vortex shedding from a circular cylinder near a moving ground. Physics of Fluids 19, 025103.
Norberg, C., 2003. Fluctuating lift on a circular cylinder: review and new measurements. Journal of Fluids and Structures 17, 57–96.
Ryan, K., Thompson, M.C., Hourigan, K., 2005. Three-dimensional transition in the wake of bluff elongated cylinders. Journal of Fluid Mechanics 538, 1–29.
Stewart, B.E., Hourigan, K., Thompson, M.C., Leweke, T., 2006. Flow dynamics and forces associated with a cylinder rolling along a wall. Physics of Fluids 18, 111701.
Stewart, B.E., Thompson, M.C., Leweke, T., Hourigan, K., 2010. The wake behind a cylinder rolling on a wall at varying rotation rates. Journal of Fluid Mechanics 648, 225–256.
Sumner, D., 2010. Two circular cylinders in cross-flow: a review. Journal of Fluids and Structures 26, 849–899.
Tan, B.T., Thompson, M.C., Hourigan, K., 2005. Evaluating fluid forces on bluff bodies using partial velocity data. Journal of Fluids and Structures 20 (1), 5–24.
Taneda, S., 1965. Experimental investigation of vortex streets. Journal of the Physical Society of Japan 20, 1714–1721.
Thompson, M.C., Hourigan, K., Cheung, A., Leweke, T., 2006a. Hydrodynamics of a particle impact on a wall. Applied Mathematical Modelling 30, 1356–1369.
Thompson, M.C., Hourigan, K., Ryan, K., Sheard, G.J., 2006b. Wake transition of two-dimensional cylinders and axisymmetric bluff bodies. Journal of Fluids and Structures 22, 793–806.
Thompson, M.C., Hourigan, K., Sheridan, J., 1996. Three-dimensional instabilities in the wake of a circular cylinder. Experimental Thermal and Fluid Science 12, 190–196.
Thompson, M.C., Leweke, T., Williamson, C.H.K., 2001. The physical mechanism of transition in bluff body wakes. Journal of Fluids and Structures 15, 607–616.
Wagner, D.D., Frenette, P.S., 2008. The vessel wall and its interactions. Blood 111, 5271–5281.
Williamson, C.H.K., 1996a. Three-dimensional wake transition. Journal of Fluid Mechanics 328, 345–407.
Williamson, C.H.K., 1996b. Vortex dynamics in the cylinder wake. Annual Review of Fluid Mechanics 28, 477–539.
Wu, J., Sheridan, J., Welsh, M.C., Hourigan, K., 1996. Three-dimensional vortex structures in a cylinder wake. Journal of Fluid Mechanics 312, 201–222.